buildings

MDPI

Article

Research on Temperature Dependence and Temperature Self-Adaptability of Laminated Rubber Isolation Bearings

Changsheng Wang *, Tao Li and Rongzheng Xu

College of Civil Engineering and Architecture, Huanghuai University, Zhumadian 463000, China; 20212184@huanghuai.edu.cn (T.L.); xurongzheng@huanghuai.edu.cn (R.X.)
* Correspondence: wangchangsheng@huanghuai.edu.cn

Abstract

As the rubber constituting laminated rubber isolation bearings is a temperature-sensitive material, its performance is susceptible to temperature disturbances. Firstly, this study systematically analyzed the effects of temperature on the mechanical properties of natural rubber bearings (LNR), lead–rubber bearings (LRB), and high–damping rubber bearings (HDR), including horizontal equivalent stiffness, equivalent damping ratio, and yield load. The variation trends of the mechanical property parameters of the three types of bearings with temperature are basically the same. LNR exhibits a strong linear variation law, while the mechanical properties of HDR bearings are the most sensitive to temperature changes. Secondly, based on the analysis of the temperature characteristics of the mechanical properties of the bearings, the temperature dependence of the seismic mitigation effect of the bearings was further studied. The results show that the displacement response of the isolation layer has the best temperature stability when using LRB bearings, and the displacement response of the superstructure is most susceptible to temperature changes when using HDR bearings. When the temperature is lower than the normal temperature, the displacement responses of isolation systems with different types of bearings all show the characteristic that the lower the temperature, the greater the deviation from the displacement response at normal temperature. Finally, to overcome the influence of temperature, a temperature-controlled isolation rubber bearing integrating laminated rubber isolation bearings with a temperature regulation system was proposed. This can solve the problems that the mechanical properties of rubber bearings deteriorate and the aging rate accelerates in a wide temperature range, which affect their isolation effect and service life. Thus, it endows new theoretical connotations to rubber isolation bearings and has practical application value for engineering seismic resistance.

Keywords: rubber isolation bearing; mechanical properties; shock absorption effect; temperature effect; temperature regulation

check for updates

Academic Editor: Harry Far

Received: 20 October 2025
Revised: 14 November 2025
Accepted: 27 November 2025
Published: 28 November 2025

Citation: Wang, C.; Li, T.; Xu, R. Research on Temperature Dependence and Temperature Self-Adaptability of Laminated Rubber Isolation Bearings. *Buildings* **2025**, *15*, 4333. https://doi.org/10.3390/buildings15234333

Copyright: © 2025 by the authors. Licensee MDPI, Basel, Switzerland. This article is an open access article distributed under the terms and conditions of the Creative Commons Attribution (CC BY) license (https://creativecommons.org/licenses/by/4.0/).

1. Introduction

Laminated rubber isolation bearings can withstand large vertical pressures while exhibiting excellent horizontal deformation capacity. These bearings reduce the seismic action on building structures by extending the natural vibration period of the structures, thereby moving them away from the characteristic period of seismic waves. Moreover, their shock absorption measures are simple and clear, with reasonable economic indicators, and post-earthquake repair is convenient. It has been more than 30 years since China applied isolation technology to building structures in 1992, and over 80% of the existing isolated

buildings adopt laminated rubber isolation bearings. Laminated rubber isolation bearings mainly include LNR, LRB, and HDR [1].

Scholars have developed a variety of constitutive models facilitating engineering applications for investigating the mechanical properties of bearings, such as the Bouc–Wen model [2], MSS model [3], Yeoh model [4], bilinear model [5], and polyline model [6]. Although commonly used bearing models take into account factors like pressure and deformation, aspects including friction effects, ambient temperature, and the evolution and deterioration mechanisms of rubber bearings during their service life still warrant further research [7,8]. Relevant studies have demonstrated that rubber isolation bearings exhibit significant temperature dependence. Temperature exerts varying degrees of influence on the vertical stiffness, horizontal stiffness, yield force, equivalent damping ratio, aging, and energy dissipation capacity of rubber bearings [9–11]. Both high-temperature environments and cyclic loading can cause an increase in the internal temperature of rubber bearings, leading to rubber softening and a certain degree of degradation in the strength and stiffness of the bearings. Low temperatures can harden the rubber, preventing it from fully demonstrating the characteristics of an elastomer, thereby affecting the deformation capacity and isolation performance of the bearings [12–14].

The application environment of current rubber bearing isolation systems is increasingly complex. For instance, heat resistance necessitates consideration in southern China, while cold resistance requires attention in northern China. It is therefore crucial to accurately characterize the temperature dependence of bearing performance and establish a design methodology for isolated structures that incorporates temperature effects. Specifications of several foreign countries have already integrated the temperature dependence of bearings into their design frameworks. In contrast, in China, when designing and analyzing isolated structures, the temperature effect is typically addressed by obtaining fixed values of mechanical parameters of isolation bearings via experimental testing, followed by introducing temperature correction coefficients.

However, for different types of rubber bearings, temperature affects their performance differently [15]. For instance, prolonged exposure of LNR to low-temperature conditions causes crystallization of natural rubber, thereby degrading its tensile strain capacity, tear resistance, and crack propagation resistance [16,17]. Although the lead core in LRB possesses superior elastoplastic behavior, the heat generated during LRB's reciprocating motion causes a temperature rise in the lead core, leading to reduced yield stress of the lead core and diminished energy dissipation capacity of the bearing. Furthermore, low-temperature hardening of lead also results in decreased energy dissipation capacity of the bearing [18–21]. In HDR, elevated temperatures reduce the hardness of graphite, reducing the frictional energy dissipation capacity between graphite molecules during horizontal shear deformation in HDR [22]. Building on this, this paper systematically analyzes the influence of temperature on the mechanical properties and isolation performance of LNR, LRB, and HDR bearings, and proposes a temperature-controlled rubber isolation bearing capable of overcoming the effects of adverse external temperatures (high temperature, low temperature, and large temperature differences) to address the issue where degraded mechanical properties of rubber isolation bearings in a broad temperature range compromise their isolation performance and service life.

2. Temperature Dependence of the Mechanical Properties of Rubber Bearings

As a temperature-sensitive material, rubber undergoes changes in its elastic modulus, shear modulus, and hardness with temperature variations [23]. Given that buildings typically have a service life exceeding 50 years, the temperature of rubber-based isolation

bearings fluctuates with seasonal temperature changes, resulting in deviations between their mechanical properties and the designed values [24,25]. Additionally, the coupling effect of vertical permanent loads and temperature can induce phenomena such as increased internal friction, deformation, hardening, aging, or cracking in rubber bearings, thereby impairing their mechanical performance, seismic mitigation effectiveness, and service life [26].

To analyze the influence of temperature on the mechanical properties of rubber bearings, scholars have derived empirical formulas convenient for designers' reference through a large number of temperature-related tests on laminated rubber isolation bearings of various specifications and models. For example, Liu et al. [27] proposed a temperature effect correction equation for the horizontal stiffness of LNR bearings.

$$K = 1.0378e^{(-0.002T)}K_{T0} \tag{1}$$

where T is the test temperature (°C); T_0 is the normal temperature of 20 °C.

Pang et al. [28] derived temperature-dependent formulas for the horizontal equivalent stiffness, post-yield stiffness, and yield load of LRB bearings.

$$K_{eq}(T) = C_{K_h}(T)K_{eq}(23\ ^\circ\mathrm{C}) \tag{2}$$

$$K_d(T) = C_{K_d}(T)K_d(23\ ^\circ\mathrm{C}) \tag{3}$$

$$Q_d(T) = C_{Q_d}(T)Q_d(23\ ^\circ\mathrm{C}) \tag{4}$$

where $C_{K_h}(T)$ is the horizontal equivalent stiffness adjustment coefficient, $C_{K_h}(T) = 1.1060\mathrm{e}^{-0.0042T}$; $C_{K_d}(T)$ is the post-yield horizontal stiffness adjustment coefficient, $C_{K_d}(T) = 0.1261\mathrm{e}^{-0.0306T} + 0.9376$; $C_{Q_d}(T)$ is the horizontal yield shear force adjustment coefficient, $C_{Q_d}(T) = 1.2140\mathrm{e}^{-0.0075T}$.

Miyamura et al. [29] presents the fitting formulas for the variation laws of the horizontal equivalent stiffness and equivalent damping ratio of HDR bearings with temperature.

$$K_{eq}(T) = C_k(T)K_{eq}(20\ ^\circ\mathrm{C}) \tag{5}$$

$$H_{eq}(T) = C_h(T)H_{eq}(20\ ^\circ\mathrm{C}) \tag{6}$$

The temperature adjustment coefficient is shown in the formula $C_k(T) = 1.0 - 0.0144(T - 20)$, $(T \le 20\ ^\circ\mathrm{C})$; $C_k(T) = 1.0 + 0.548\left[\log_{10}(20 - 3.45) - \log_{10}(T - 3.45)\right]$, $(T > 20\ ^\circ\mathrm{C})$; $C_h(T) = 1.0 - 0.0065(T - 20)$.

Shen et al. [30] and Jin et al. [31] analyzed the variation laws of horizontal equivalent stiffness, equivalent damping ratio, yield load, and post–yield horizontal stiffness of LNR, LRB, and HDR bearings with temperature through compression–shear tests under different temperature conditions. However, a comparative analysis on the extent to which temperature affects the mechanical properties of different types of laminated rubber isolation bearings has not been reported. Through a systematic review, Figure 1 presents the ratios of the mechanical properties of LNR, LRB, and HDR bearings under different temperature conditions to those at the normal temperature of 23 °C.

A comparative analysis reveals that the horizontal equivalent stiffness of HDR is most significantly affected by temperature, while that of LNR is the least affected. The equivalent damping ratios of both LNR and HDR decrease with increasing temperature. A reduction in the bearing damping ratio will lead to a decrease in its energy dissipation capacity, thereby weakening the bearing's effect on dissipating seismic energy and further increasing the displacement response of the superstructure. In contrast, the equivalent damping ratio of LRB exhibits minimal variation with temperature, which can be neglected.

Temperature exerts a substantial influence on the yield load and post-yield stiffness of HDR. For LNR and LRB, the effects of temperature on their yield loads and post-yield stiffness are comparable and cannot be ignored.

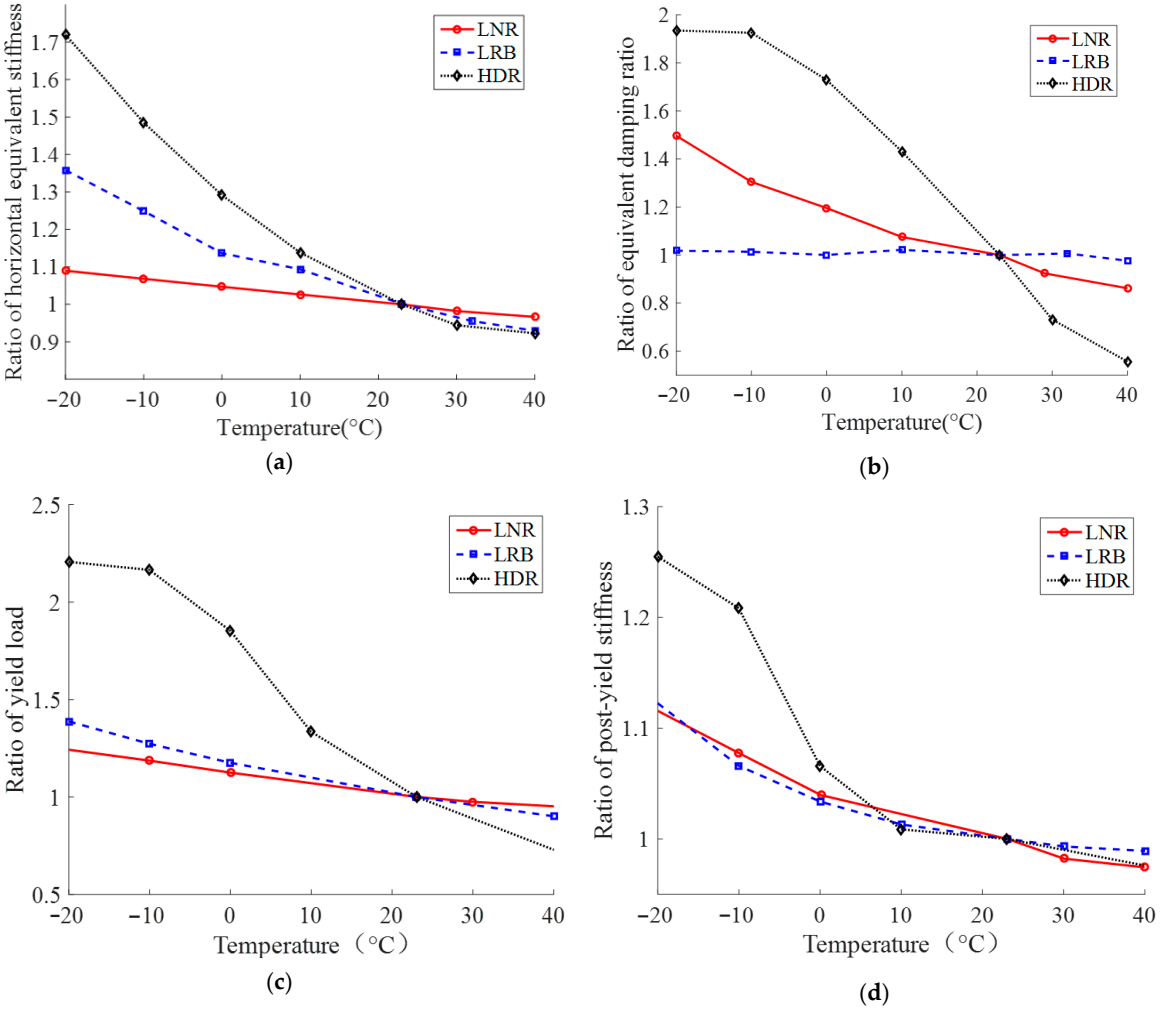


Figure 1. Ratio of mechanical properties at each temperature to 23 °C: (**a**) horizontal equivalent stiffness; (**b**) equivalent damping ratio; (**c**) yield load; (**d**) post-yield stiffness.

From a micro-level perspective, the damping effect of HDR mainly originates from the frictional energy dissipation at the interface between rubber molecular chains and filler particles. Under low-temperature conditions, the movement of molecular chains in the material is restricted, leading to increased brittleness and reduced energy dissipation capacity. Under high-temperature conditions, the excessive activity of molecular chains weakens the interfacial interaction, resulting in a simultaneous decrease in the storage modulus and loss factor, which manifests as softening and attenuation of damping efficiency. The rubber in LRB mainly provides elastic restoring force; although it exhibits slight viscous damping itself, the lead core plays a dominant role in the overall mechanical behavior of LRB, and the damping of LRB is mainly achieved through the deformation of the lead core. Therefore, LRB exhibits better thermal stability than HDR.

3. Temperature Dependence of the Seismic Reduction Effect of Rubber Bearings

The deformation of isolation bearings in the isolation layer is directly related to the isolation performance of the isolated structure [32]. The variation in the mechanical properties

of rubber isolation bearings with temperature inevitably leads to a corresponding change in their seismic reduction effect with temperature. On the basis of the aforementioned discussion on the temperature dependence of the mechanical properties of bearings, this section analyzes the temperature dependence of their seismic reduction effect.

3.1. Analytical Solution for Displacement Response of Isolated Structures

A two-degree-of-freedom base-isolated structure model is selected to analyze the influence of temperature on the seismic reduction effect of rubber bearings. The superstructure is simplified into an equivalent mass point, which, together with a mass point in the isolation layer, forms a two-degree-of-freedom model. The analytical model is shown in Figure 2.

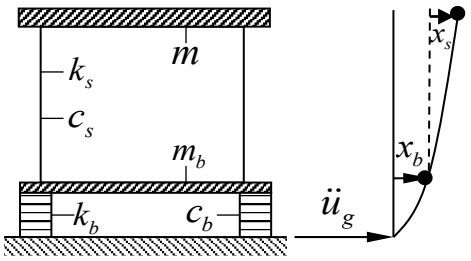


Figure 2. Isolation structure equivalent system.

In the figure, k_s, c_s, and m represent the stiffness, damping, and mass of the superstructure after equivalent treatment of the original system, respectively. k_b, c_b, and m_b denote the stiffness, damping, and mass of the isolation layer, respectively, where the stiffness and damping of the isolation layer are variables that change with temperature. Let x_b and x_s denote the displacement of the isolation layer relative to the ground and the displacement of the superstructure relative to the isolation layer, respectively. Then, under the action of ground motion $\ddot{u}_g(t)$, the equation of motion of the structure is established by means of dynamic equilibrium as follows:

$$\begin{cases} (m_b + m)\ddot{x}_b(t) + m\ddot{x}_s(t) + c_b(T)\dot{x}_b(t) + k_b(T)x_b(t) = -(m_b + m)\ddot{u}_g(t) \\ m\ddot{x}_b(t) + m\ddot{x}_s(t) + c_s\dot{x}_s(t) + k_s x_s(t) = -m\ddot{u}_g(t) \end{cases} \tag{7}$$

The equation of motion (7) is expressed in matrix form as $\boldsymbol{M}\ddot{\boldsymbol{x}}(t) + \boldsymbol{C}\dot{\boldsymbol{x}}(t) + \boldsymbol{K}\boldsymbol{x}(t) = -\boldsymbol{M}\boldsymbol{r}\ddot{u}_g(t)$, where $\boldsymbol{M} = \begin{bmatrix} m_b + m & m \\ m & m \end{bmatrix}$, $\boldsymbol{C} = \begin{bmatrix} c_b(T) & 0 \\ 0 & c_s \end{bmatrix}$, $\boldsymbol{K} = \begin{bmatrix} k_b(T) & 0 \\ 0 & k_s \end{bmatrix}$, $\boldsymbol{x}(t) = \begin{Bmatrix} x_b(t) \\ x_s(t) \end{Bmatrix}$, $\boldsymbol{r} = \begin{Bmatrix} 1 \\ 0 \end{Bmatrix}$.

The structural displacement response is expressed by the mode shape vector $\boldsymbol{\varphi}_i$ and the generalized coordinate $q_i(t)$. Through the coordinate transformation formula $\boldsymbol{x}(t) = \sum_{i=1}^{2} \boldsymbol{\varphi}_i q_i(t)$, the following can be obtained:

$$\ddot{q}_1(t) + 2\omega_1\xi_1\dot{q}_1(t) + \lambda_1\dot{q}_2(t) + {\omega_1}^2 q_1(t) = -L_1\ddot{u}_g(t) \tag{8}$$

$$\ddot{q}_2(t) + \lambda_2\dot{q}_1(t) + 2\omega_2\xi_2\dot{q}_2(t) + {\omega_2}^2 q_2(t) = -L_2\ddot{u}_g(t) \tag{9}$$

The frequency ω_i, damping ratio ξ_i, and parameters λ_i and L_i in the formula can be obtained by the following expressions: ${\boldsymbol{\varphi}_i}^T\boldsymbol{M}\boldsymbol{\varphi}_i = M_i$, $M_i 2\omega_i\xi_i = {\boldsymbol{\varphi}_i}^T\boldsymbol{C}\boldsymbol{\varphi}_i$, $M_i{\omega_i}^2 = {\boldsymbol{\varphi}_i}^T\boldsymbol{K}\boldsymbol{\varphi}_i$, $\lambda_1 M_1 = {\boldsymbol{\varphi}_1}^T\boldsymbol{C}\boldsymbol{\varphi}_2$, $\lambda_2 M_2 = {\boldsymbol{\varphi}_2}^T\boldsymbol{C}\boldsymbol{\varphi}_1$, $L_i = {\boldsymbol{\varphi}_i}^T\boldsymbol{M}\boldsymbol{r}/M_i$ $(i = 1, 2)$.

We express Equations (8) and (9) in matrix form:

$$\ddot{\boldsymbol{q}}(t) + \boldsymbol{D}\dot{\boldsymbol{q}}(t) + \boldsymbol{R}\boldsymbol{q}(t) = \boldsymbol{p}(t) \tag{10}$$

The matrix $\boldsymbol{D}$ in the above formula satisfies $\boldsymbol{D} = \begin{bmatrix} 2\omega_1\xi_1 & \lambda_1 \\ \lambda_2 & 2\omega_2\xi_2 \end{bmatrix}$, with $\boldsymbol{R} = \mathrm{diag}[{\omega_1}^2, {\omega_2}^2]$ and $\boldsymbol{p}(t) = [-L_1, -L_2]^{\mathrm{T}}\ddot{u}_g(t)$.

Let $\boldsymbol{D} = \boldsymbol{\Lambda} + \varepsilon\boldsymbol{D}_0$, where matrix $\boldsymbol{\Lambda} = \mathrm{diag}[2\omega_1\xi_1, 2\omega_2\xi_2]$ and $\boldsymbol{D}_0 = \boldsymbol{D} - \boldsymbol{\Lambda} = \begin{bmatrix} 0 & \lambda_1 \\ \lambda_2 & 0 \end{bmatrix}$. When the parameter $\varepsilon = 0$, it indicates that the influence of the damping velocity coupling term on the system is not considered; when $\varepsilon = 1$, the system reverts to the original one. Substituting $\boldsymbol{D} = \boldsymbol{\Lambda} + \varepsilon\boldsymbol{D}_0$ into Equation (4), we can obtain

$$\ddot{\boldsymbol{q}}(t) + \boldsymbol{\Lambda}\dot{\boldsymbol{q}}(t) + \boldsymbol{R}\boldsymbol{q}(t) = \boldsymbol{p}(t) - \varepsilon\boldsymbol{D}_0\dot{\boldsymbol{q}}(t) \tag{11}$$

The perturbation method is employed to solve Equation (11). Let the solution of Equation (11) be $\boldsymbol{q}(t) = \boldsymbol{q}^{(1)}(t) + \varepsilon\boldsymbol{q}^{(2)}(t)$; then, according to the coefficients of the same power of ε, the following can be obtained:

$$\ddot{\boldsymbol{q}}^{(1)}(t) + \boldsymbol{\Lambda}\dot{\boldsymbol{q}}^{(1)}(t) + \boldsymbol{R}\boldsymbol{q}^{(1)}(t) = \boldsymbol{p}(t) \tag{12}$$

$$\ddot{\boldsymbol{q}}^{(2)}(t) + \boldsymbol{\Lambda}\dot{\boldsymbol{q}}^{(2)}(t) + \boldsymbol{R}\boldsymbol{q}^{(2)}(t) = -\boldsymbol{D}_0\dot{\boldsymbol{q}}^{(1)}(t) \tag{13}$$

$\boldsymbol{q}^{(1)}(t)$ is obtained from matrix Equation (6). Treating $-\boldsymbol{D}_0\dot{\boldsymbol{q}}^{(1)}(t)$ as the excitation vector, the solution of $\boldsymbol{q}^{(2)}(t)$ can be derived. From matrix Equations (12) and (13), the following is obtained:

$$\begin{Bmatrix} \ddot{q}_1{}^{(1)}(t) \\ \ddot{q}_2{}^{(1)}(t) \end{Bmatrix} + \begin{bmatrix} 2\omega_1\xi_1 & 0 \\ 0 & 2\omega_2\xi_2 \end{bmatrix} \begin{Bmatrix} \dot{q}_1{}^{(1)}(t) \\ \dot{q}_2{}^{(1)}(t) \end{Bmatrix} + \begin{bmatrix} {\omega_1}^2 & 0 \\ 0 & {\omega_2}^2 \end{bmatrix} \begin{Bmatrix} q_1{}^{(1)}(t) \\ q_2{}^{(1)}(t) \end{Bmatrix} = -\begin{Bmatrix} L_1 \\ L_2 \end{Bmatrix} \ddot{u}_g(t) \tag{14}$$

$$\begin{Bmatrix} \ddot{q}_1{}^{(2)}(t) \\ \ddot{q}_2{}^{(2)}(t) \end{Bmatrix} + \begin{bmatrix} 2\omega_1\xi_1 & 0 \\ 0 & 2\omega_2\xi_2 \end{bmatrix} \begin{Bmatrix} \dot{q}_1{}^{(2)}(t) \\ \dot{q}_2{}^{(2)}(t) \end{Bmatrix} + \begin{bmatrix} {\omega_1}^2 & 0 \\ 0 & {\omega_2}^2 \end{bmatrix} \begin{Bmatrix} q_1{}^{(2)}(t) \\ q_2{}^{(2)}(t) \end{Bmatrix} = -\begin{bmatrix} 0 & \lambda_1 \\ \lambda_2 & 0 \end{bmatrix} \begin{Bmatrix} \dot{q}_1{}^{(1)}(t) \\ \dot{q}_2{}^{(1)}(t) \end{Bmatrix} \tag{15}$$

By performing Laplace transform and inverse Laplace transform on Equations (14) and (15), the following can be obtained:

$$q_1{}^{(1)}(t) = L_1\delta_1(t) \tag{16}$$

$$q_2{}^{(1)}(t) = L_2\delta_2(t) \tag{17}$$

$$q_1{}^{(2)}(t) = -\lambda_1 L_2\left[a\delta_1(t) + b\dot{\delta}_1(t) + c\delta_2(t) + d\dot{\delta}_2(t)\right] \tag{18}$$

$$q_2{}^{(2)}(t) = -\lambda_2 L_1\left[a\delta_1(t) + b\dot{\delta}_1(t) + c\delta_2(t) + d\dot{\delta}_2(t)\right] \tag{19}$$

In the formula, $\delta_j(t) = -\frac{1}{\overline{\omega}_j}\int_0^t \ddot{u}_g(\tau)e^{-\xi_j\omega_j(t-\tau)}\sin\overline{\omega}_j(t-\tau)d\tau$ and $\overline{\omega}_j = \omega_j\sqrt{1-{\xi_j}^2}$ $(j = 1, 2)$. The coefficients are $a = {\omega_1}^2(2\omega_2\xi_2 - 2\omega_1\xi_1)/E$, $b = ({\omega_2}^2 - {\omega_1}^2)/E$, $c = -{\omega_2}^2(2\omega_2\xi_2 - 2\omega_1\xi_1)/E$, $d = -({\omega_2}^2 - {\omega_1}^2)/E$ and $E = ({\omega_2}^2 - {\omega_1}^2)^2 + (2\omega_2\xi_2 - 2\omega_1\xi_1) \times ({\omega_1}^2 2\omega_2\xi_2 - {\omega_2}^2 2\omega_1\xi_1)$.

From $q_n(t) = q_n{}^{(1)}(t) + \varepsilon q_n{}^{(2)}(t)$, let $\varepsilon = 1$. Combined with the coordinate transformation formula $\boldsymbol{x(t)} = \boldsymbol{\varphi q(t)}$, we can obtain

$$x_n = \sum_{k=1}^{2} a_{nk}\delta_k(t) + b_{nk}\dot{\delta}_k(t);\ (n = 1, 2) \tag{20}$$

In Equation (20), the coefficients are $a_{n1} = (L_1 - a\lambda_1 L_2)\varphi_{n1} - a\lambda_2 L_1 \varphi_{n2}$, $a_{n2} = -c\lambda_1 L_2 \varphi_{n1} + (L_2 - c\lambda_2 L_1)\varphi_{n2}$, $b_{n1} = -b\lambda_1 L_2 \varphi_{n1} - b\lambda_2 L_1 \varphi_{n2}$, and $b_{n2} = -d\lambda_1 L_2 \varphi_{n1} - d\lambda_2 L_1 \varphi_{n2}$.

3.2. Example of Temperature Dependence of Bearing Vibration Reduction Effect

We analyze the influence of temperature on the damping effects of LNR, LRB and HDR. A two-degree-of-freedom base-isolated structure was selected as the analytical model, with the superstructure parameters specified as follows: mass $m = 8.5 \times 10^5$ kg, stiffness $k_s = 1.5 \times 10^9$ N/m, and damping ratio $\zeta_s = 0.05$. The isolation layer was assigned a mass of $m_b = 2.2 \times 10^5$ kg. The engineering is designed with a seismic fortification intensity of 8 degrees, belonging to the second group of design earthquake groups, constructed on type II site soil, and analyzed according to rare earthquakes. An artificial ground motion was generated based on the code-specified acceleration response spectrum, and its validity was confirmed by comparing its acceleration response spectrum with the code requirements. The input seismic waves included the El Centro wave, Taft wave, and the aforementioned artificial wave, each scaled to a peak acceleration of 400 cm/s^2. The verification results for the input waves and the artificial wave are illustrated in Figure 3.

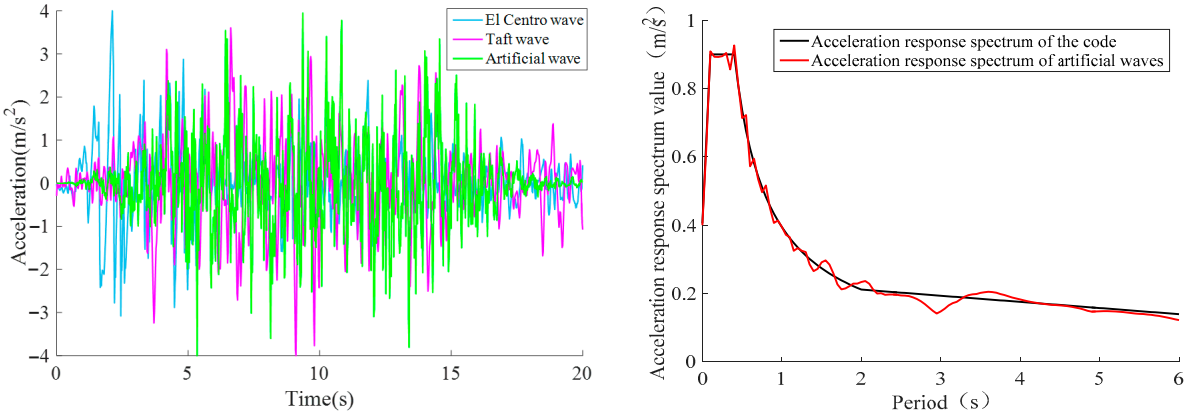


Figure 3. Input seismic waves and verification of artificial waves: (**a**) input seismic wave; (**b**) comparison of response spectra.

Given the stiffness and damping ratio of various types of isolation layers at the ambient temperature of 23 °C, and in conjunction with the aforementioned ratios of the horizontal equivalent stiffness and equivalent damping ratio of LNR, LRB, and HDR under different temperature conditions to those at 23 °C, the stiffness and damping ratios of the isolation layers at −20 °C, −10 °C, 0 °C, and 40 °C are presented in Table 1.

Table 1. Stiffness and damping ratios of isolation layers of various types of supports under different temperature conditions.

Mechanical Properties	Bearing Type	−20 °C	−10 °C	0 °C	23 °C	40 °C
Horizontal stiffness ($\times 10^7$ N/m)	LNR	0.87	0.85	0.84	0.80	0.77
	LRB	1.63	1.50	1.36	1.20	1.11
	HDR	2.24	1.93	1.68	1.30	1.20
Damping ratio	LNR	0.15	0.13	0.12	0.10	0.08
	LRB	0.23	0.22	0.22	0.22	0.21
	HDR	0.39	0.38	0.35	0.20	0.11

A time-history analysis of the displacement response of the base-isolated structure was conducted. LNR, LRB, and HDR bearings were adopted respectively. When El Centro

wave, Taft wave, and artificial wave were used as external excitations, the time histories of displacement responses of the isolation layer and superstructure under the working conditions of −20 °C, −10 °C, 0 °C, 23 °C, and 40 °C are shown in Figures 4–6.

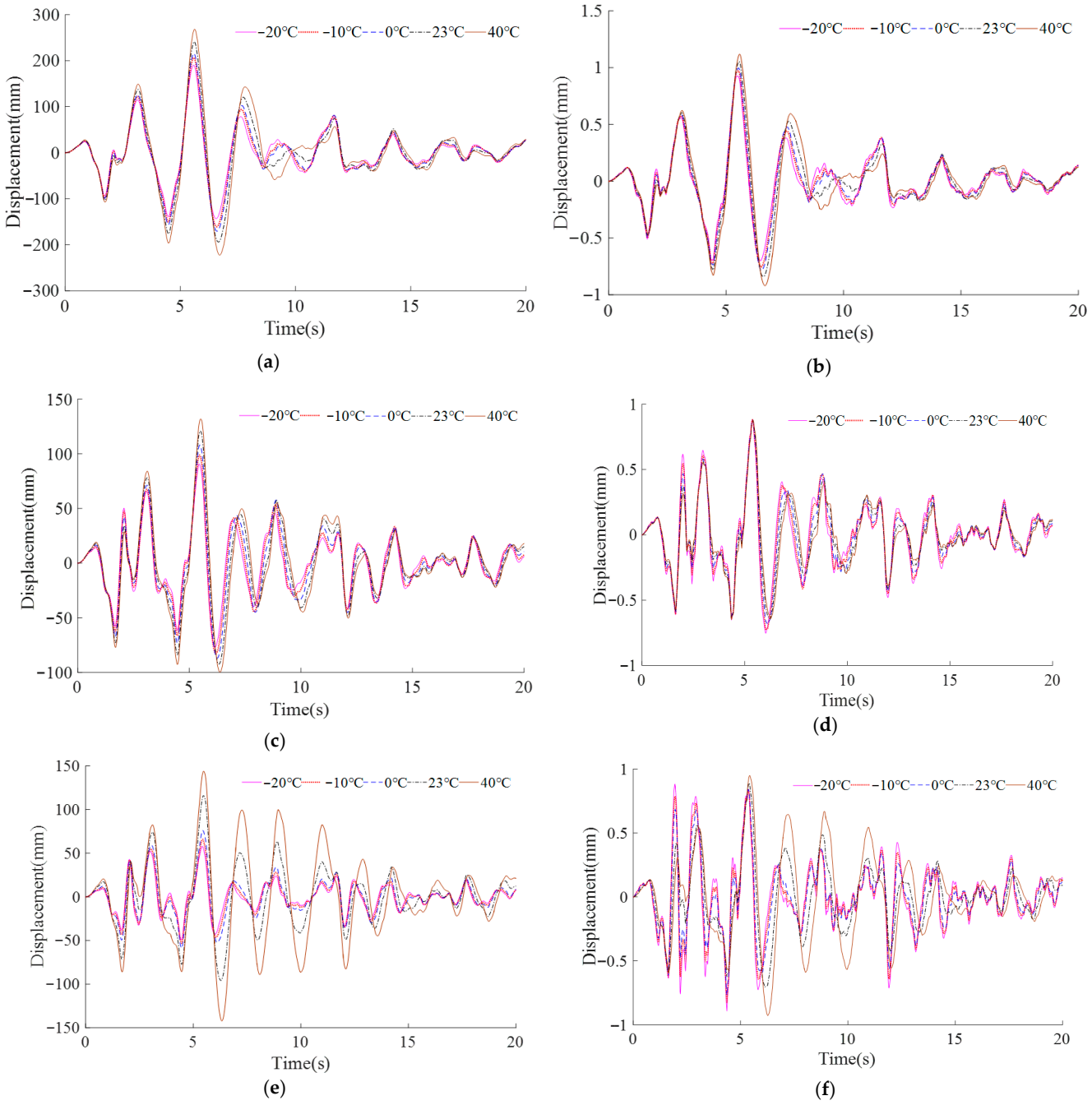


Figure 4. Responses of isolation layers and superstructures using LNR, LRB and HDR bearings under El Centro wave action: (**a**) response of the isolation layer when using LNR bearings; (**b**) response of the superstructure when using LNR bearings; (**c**) response of the isolation layer when using LRB bearings; (**d**) response of the superstructure when using LRB bearings; (**e**) response of the isolation layer when using HDR bearings; (**f**) response of the superstructure when using HDR bearings.

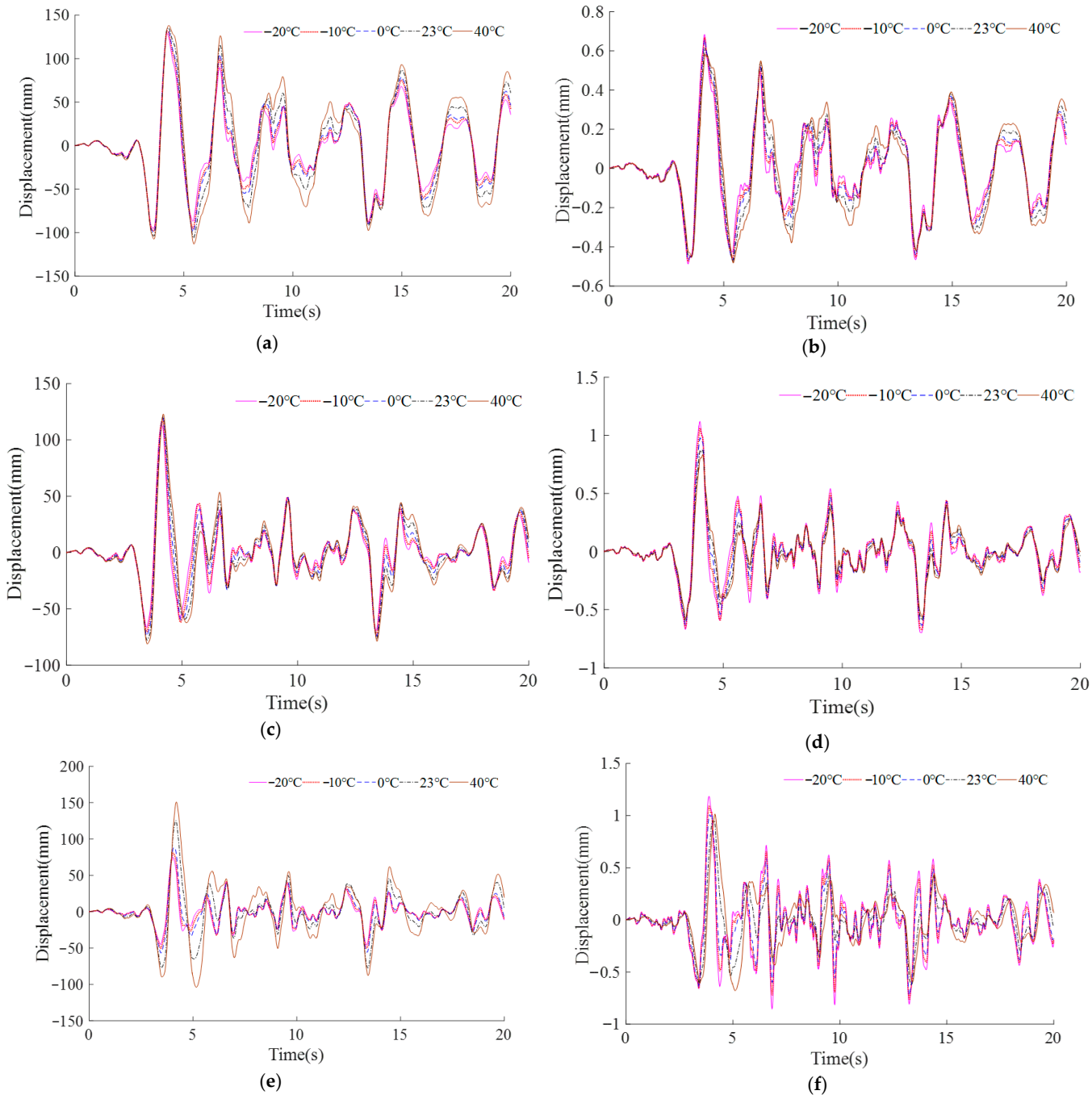


Figure 5. Responses of isolation layers and superstructures using LNR, LRB and HDR bearings under Taft wave action: (**a**) response of the isolation layer when using LNR bearings; (**b**) response of the superstructure when using LNR bearings; (**c**) response of the isolation layer when using LRB bearings; (**d**) response of the superstructure when using LRB bearings; (**e**) response of the isolation layer when using HDR bearings; (**f**) response of the superstructure when using HDR bearings.

As can be seen from the time-history curves, temperature exerts a significant influence on the seismic response of isolated structures, and neglecting temperature factors will lead to distortion in the dynamic response of isolated structures. Meanwhile, the displacement responses of the isolation system under the excitation of the three seismic waves show consistent results: the displacement response of the HDR bearing isolation system exhibits the largest fluctuation due to temperature, followed by the LNR bearing isolation system, while the LRB bearing isolation system is the least affected by temperature. Figures 7–9 present a comparative analysis of the maximum displacement responses of the isolation

layer and superstructure with different types of bearings at various temperatures under the action of El Centro wave, Taft wave, and artificial wave. The calculation results of the peak accelerations of the isolation layer and the superstructure as a function of temperature are presented in Figures 10–12.

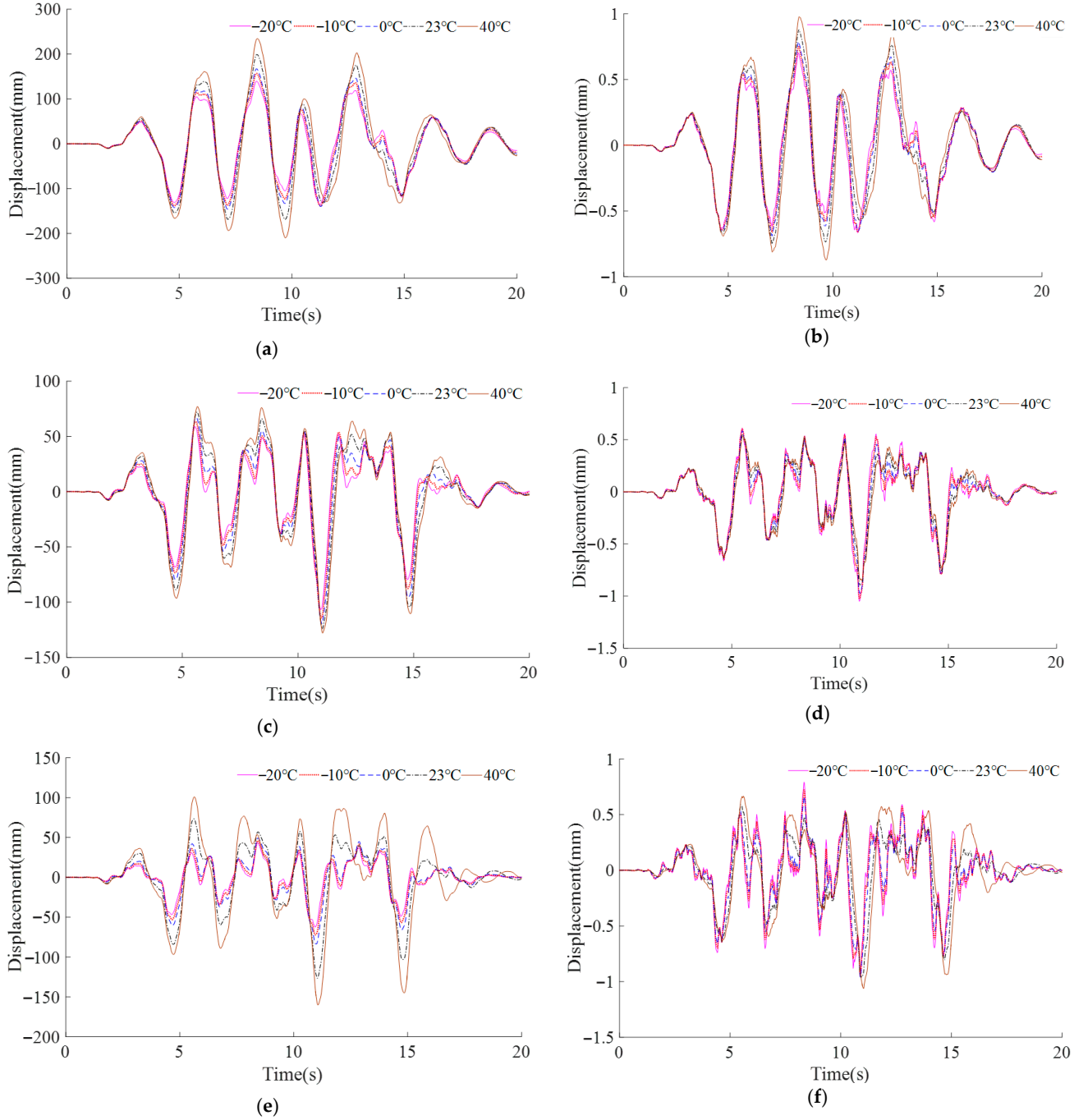


Figure 6. Responses of isolation layers and superstructures using LNR, LRB and HDR bearings under artificial wave action: (**a**) response of the isolation layer when using LNR bearings; (**b**) response of the superstructure when using LNR bearings; (**c**) response of the isolation layer when using LRB bearings; (**d**) response of the superstructure when using LRB bearings; (**e**) response of the isolation layer when using HDR bearings; (**f**) response of the superstructure when using HDR bearings.

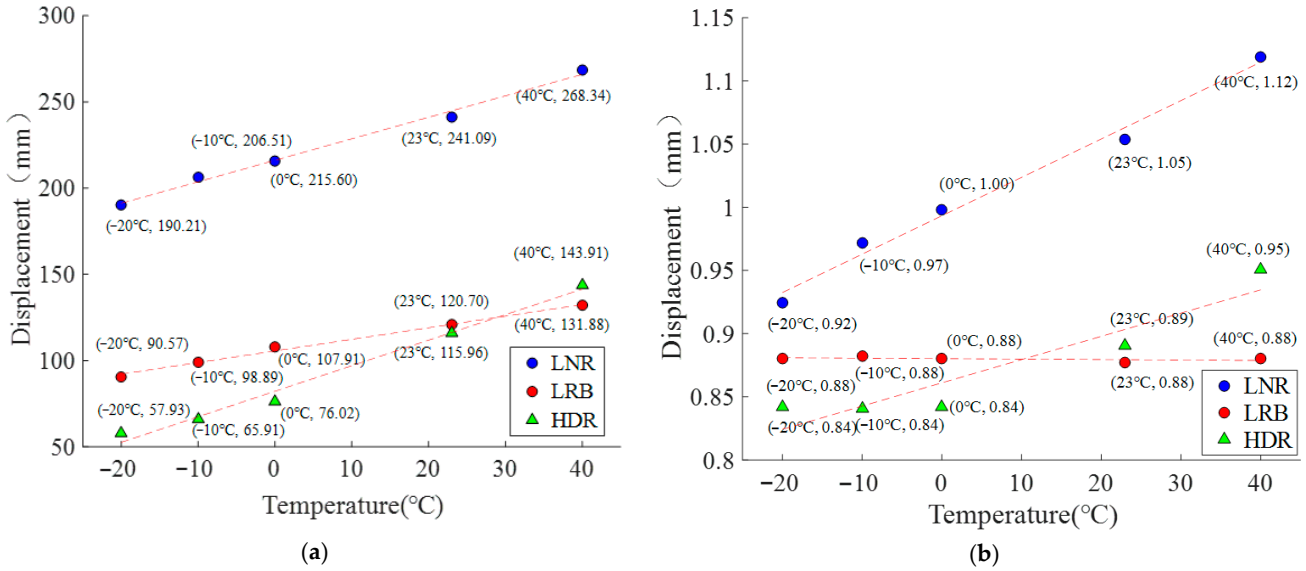


Figure 7. Comparison of maximum displacement responses under the action of El Centro wave: (**a**) comparison of displacement responses of isolation layers; (**b**) comparison of displacement responses of superstructures.

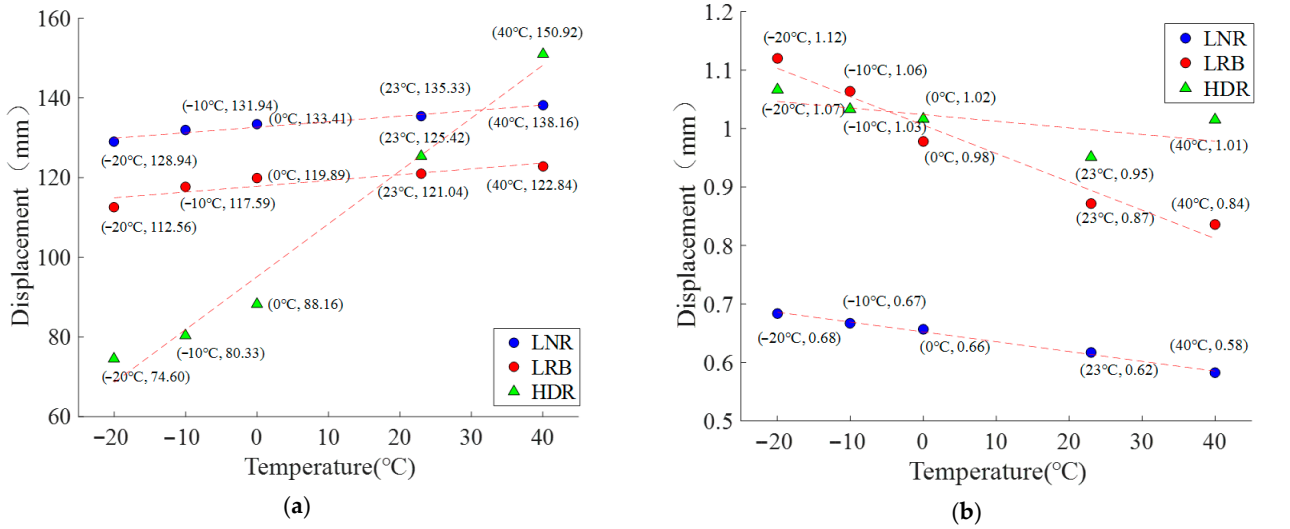


Figure 8. Comparison of maximum displacement responses under the action of Taft wave: (**a**) comparison of displacement responses of isolation layers; (**b**) comparison of displacement responses of superstructures.

As demonstrated by comparative analysis, the variation trends under the action of different seismic waves are essentially consistent. The maximum displacement of the isolation layer with LNR bearings increases approximately linearly with rising temperature, which is consistent with the approximate linear decrease in the horizontal equivalent stiffness of LNR bearings as temperature increases. When LRB bearings are adopted, the maximum displacement of the isolation layer increases with temperature elevation, while the fluctuation is relatively small. In contrast, the maximum displacement response of the isolation layer with HDR bearings exhibits a non-linear increase as temperature rises. Specifically, the maximum deviation of the maximum displacement of the LNR bearing isolation layer between −20 °C and normal temperature (23 °C) is 29.97%, that of LRB bearings is 24.96%, and that of HDR bearings reaches 50.83%. When comparing 40 °C with normal temperature (23 °C), the maximum deviation of the maximum displacement of the LNR bearing isolation layer is 17.67%, that of LRB bearings is 9.26%, and that of HDR

bearings is 26.37%. Furthermore, comparative analysis of the maximum acceleration of the isolation system indicates that as temperature decreases, the stiffness of the isolation bearings increases. This leads to the attenuation of the isolation effect and the amplification of the acceleration response of the superstructure, which underscores the necessity of considering the temperature effect in the design of isolation systems under extreme climatic conditions.

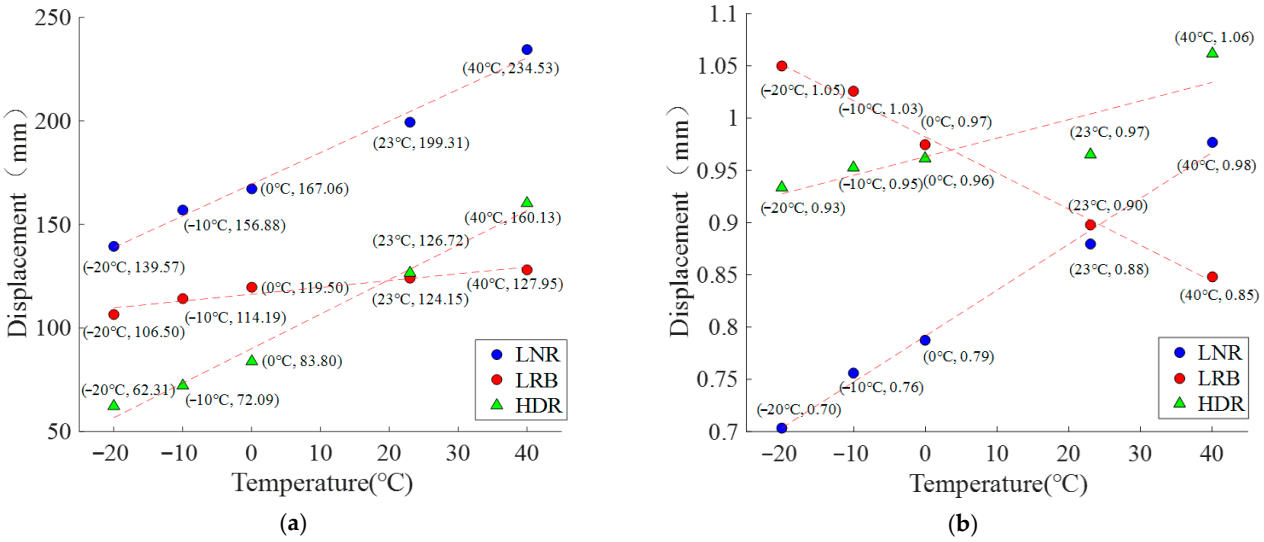


Figure 9. Comparison of maximum displacement responses under the action of artificial waves: (**a**) comparison of displacement responses of isolation layers; (**b**) comparison of displacement responses of superstructures.

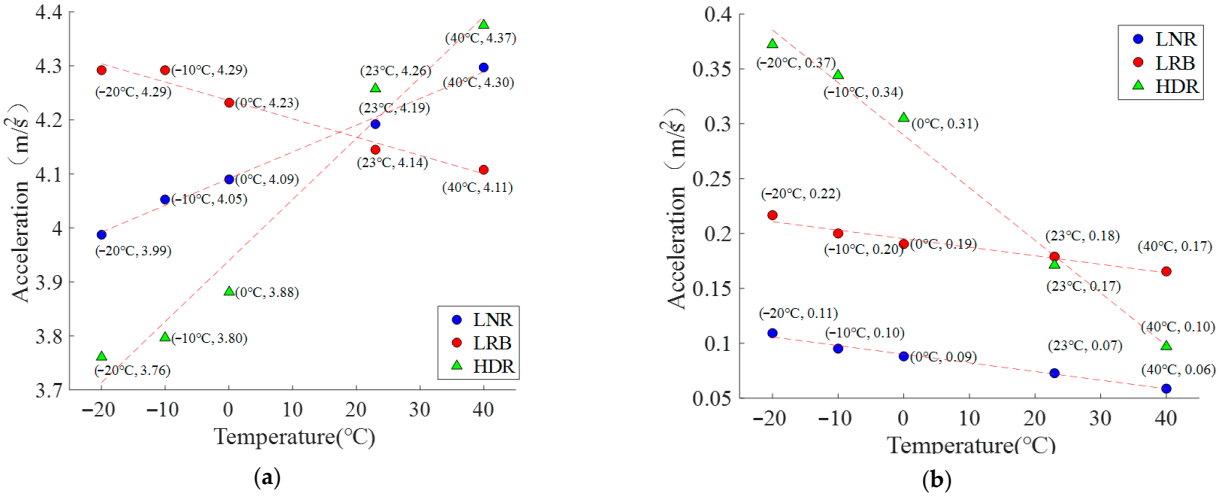
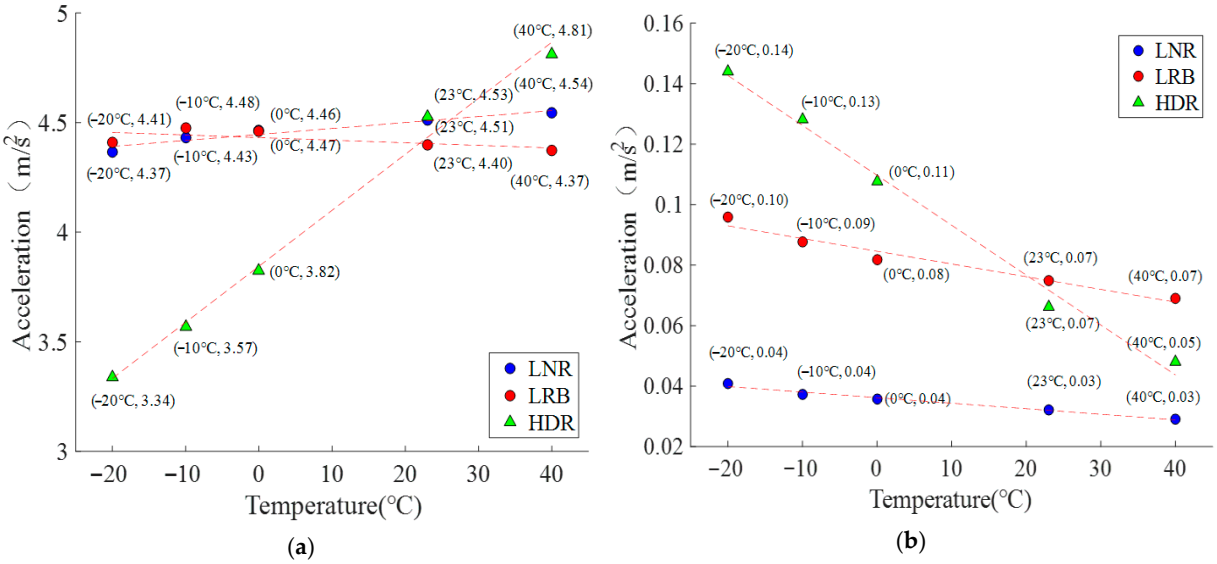


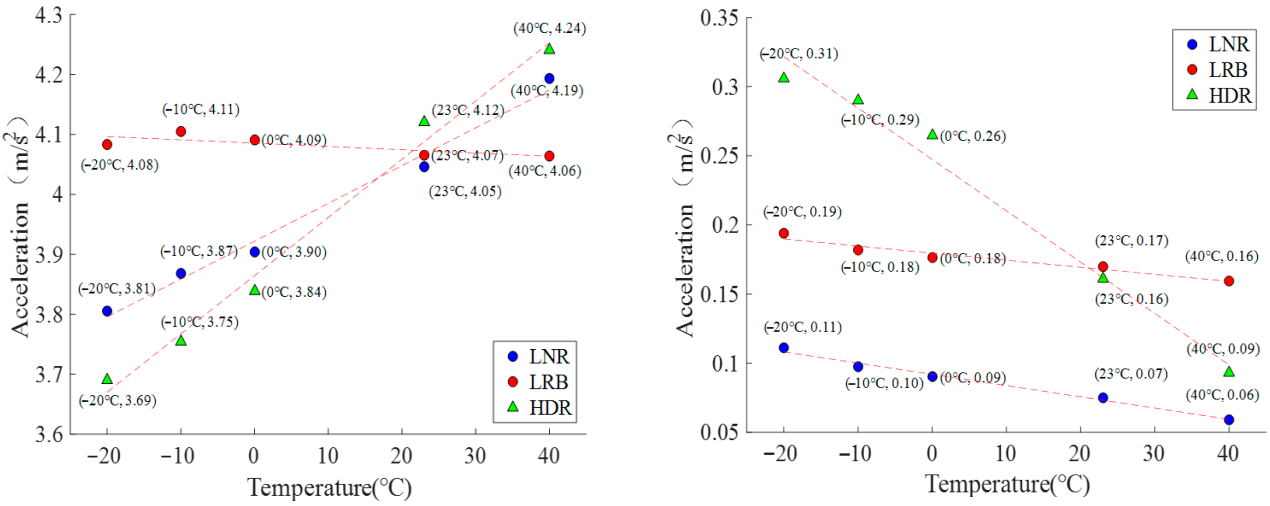
Figure 10. Comparison of peak acceleration under the action of El Centro wave: (**a**) comparison of peak acceleration of isolation layers; (**b**) comparison of peak acceleration of the superstructure.

The root mean square (RMS) differences in displacement response time histories between the isolation layer and superstructure with different types of isolation bearings at −20 °C, −10 °C, 0 °C, 40 °C and the ambient temperature of 23 °C under the action of El Centro wave, Taft wave and artificial wave were calculated. The results are presented in Tables 2–4.



(**a**) (**b**)

Figure 11. Comparison of peak acceleration under the action of Taft wave: (**a**) comparison of peak acceleration of isolation layers; (**b**) comparison of peak acceleration of the superstructure.



(**a**) (**b**)

Figure 12. Comparison of peak acceleration under the action of artificial waves: (**a**) comparison of peak acceleration of isolation layers; (**b**) comparison of peak acceleration of the superstructure.

Table 2. The root mean square difference between different temperatures and 23 °C (El Centro wave).

Location	Bearing Type	−20 °C	−10 °C	0 °C	40 °C
Isolation layer	LNR	23.82	17.45	13.72	15.82
	LRB	16.50	12.90	7.67	5.72
	HDR	23.78	20.80	17.10	21.56
Superstructure	LNR	0.11	0.08	0.06	0.07
	LRB	0.12	0.09	0.05	0.03
	HDR	0.22	0.19	0.15	0.15

Table 3. The root mean square difference between different temperatures and 23 °C (Taft wave).

Location	Bearing Type	−20 °C	−10 °C	0 °C	40 °C
Isolation layer	LNR	16.22	11.71	9.12	10.04
	LRB	12.73	9.72	5.64	4.11
	HDR	19.75	17.06	13.82	14.98
Superstructure	LNR	0.07	0.05	0.04	0.04
	LRB	0.10	0.07	0.04	0.02
	HDR	0.22	0.18	0.14	0.11

Table 4. The root mean square difference between different temperatures and 23 °C (artificial wave).

Location	Bearing Type	−20 °C	−10 °C	0 °C	40 °C
Isolation layer	LNR	26.97	19.87	15.70	18.80
	LRB	16.53	12.88	7.72	5.92
	HDR	23.88	20.60	16.63	18.82
Superstructure	LNR	0.12	0.08	0.07	0.07
	LRB	0.10	0.07	0.04	0.03
	HDR	0.20	0.17	0.13	0.12

Calculations under different seismic excitations indicate that when the temperature is lower than the normal temperature, the LNR, LRB, and HDR bearings all exhibit a trend: the lower the temperature, the greater the deviation of their responses from those at normal temperature. Among them, the LRB bearings show the smallest deviation in the displacement response of the isolation layer compared with that at normal temperature, while the isolation system using HDR bearings exhibits the largest deviation in displacement response from that at normal temperature.

4. Seismic Isolation Bearing Schemes to Overcome Temperature Effects

Given that the influence of temperature on the performance of rubber bearings cannot be neglected, it is necessary to develop new types of elastomeric isolation bearings with low temperature sensitivity to avoid the impact of ambient temperature variations.

4.1. Proposal of Temperature-Controlled Rubber Isolation Bearings

The temperature-controlled rubber isolation bearing (the schematic diagram is shown in Figure 13) is composed of an ordinary laminated rubber isolation bearing and a temperature regulation system. The temperature regulation system is made up of components such as a compressor, a condenser, a throttling device and an evaporator. By using the temperature regulation system to control the working temperature of the laminated rubber isolation bearing, the rubber bearing can achieve good temperature adaptability. It can avoid the problems that under low-temperature conditions, the rubber bearing becomes brittle, its elasticity decreases, and its stiffness increases, which leads to the shortening of the natural vibration period of the isolation structure. As a result, the isolation structure may fail to effectively avoid the main frequency band of the earthquake, the risk of resonance increases, the damping performance of the bearing decreases and the failure probability of the isolation structure rises. At the same time, it solves the problems that under high-temperature conditions, the strength and stiffness decay, the bearing deforms or fails due to aging, the softening of rubber materials accelerates, and the horizontal restoring force of the bearing decreases, which easily causes residual deformation and weakens the isolation effect.

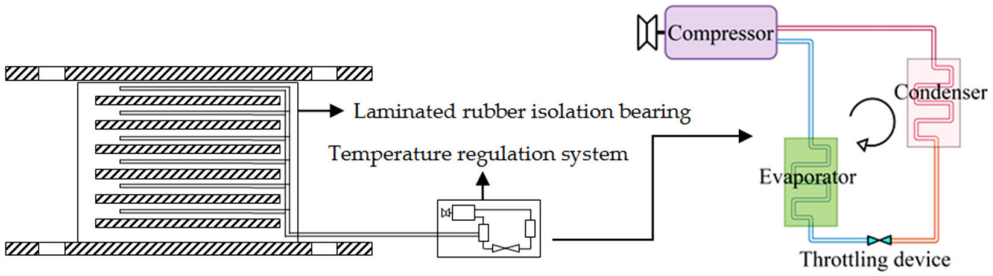


Figure 13. Schematic diagram of temperature-controlled rubber isolation bearing.

4.2. Temperature Regulation Mechanism

When the temperature of the bearing exceeds the threshold, the temperature regulation system is activated. The high-temperature and high-pressure gaseous refrigerant discharged from the compressor flows into the condenser, where it is converted into a high-temperature and high-pressure liquid refrigerant after passing through the condenser. Upon passing through the throttling device, the refrigerant turns into a low-temperature and low-pressure liquid, which then flows into the evaporator coil (refrigerant coil) embedded within the bearing to cool the rubber isolation bearing. After absorbing heat from the rubber bearing, the refrigerant is transformed into a low-temperature and low-pressure gaseous state and flows back to the compressor, thus completing the refrigeration cycle. When the bearing temperature is too low and heating is required, the four-way valve in the temperature control system reverses the flow direction of the refrigerant, and the refrigerant coil is converted into a heating medium coil to raise the temperature of the rubber isolation bearing.

4.3. Key Implementation Points for Temperature-Controlled Rubber Isolation Bearings

(1) The connection method between the rubber bearing and the temperature control device should be reasonably determined to avoid affecting the integrity of the rubber isolation bearing while ensuring efficient heat transfer, enabling the cold and heat medium coils arranged inside the bearing to deform synergistically with the bearing.

(2) Based on analyzing the influence of temperature on the mechanical properties and seismic isolation effect of rubber bearings, the ideal operating temperature value of rubber isolation bearings should be determined, and the temperature control system should be used to stabilize the operating temperature of the bearings within the ideal range. A reasonable temperature dead zone should be set to avoid frequent start-up and shutdown of the compressor in the temperature control system. Moreover, when the power supply to the temperature regulation system is cut off, the temperature-controlled rubber isolation bearing is converted into an ordinary rubber isolation bearing, which still maintains the seismic isolation effect.

(3) Refrigerants with high thermal conductivity, large refrigerating capacity per unit volume, low viscosity, and low density should be selected to improve the cooling and heating coefficients of the temperature regulation system. In combination with the bearing size, operating environment, and reasonable settings of the rubber bearing's operating temperature and condensation mode, low power consumption of the temperature regulation system can be achieved.

(4) When multiple bearings share a single temperature control system, it is necessary to address the issues of dynamic balanced distribution and collaborative intelligent control in multi-branch thermal systems. By implementing collaborative and precise regulation of temperature variations across different branches, the thermal reliability of all bearings can be ensured while reducing energy consumption. During non-seismically active periods and when temperatures are moderate, the temperature

control system is automatically switched to a low-power dormant or intermittent operation mode, thereby achieving energy conservation to the greatest extent possible.

5. Conclusions

In this paper, the temperature dependence of the mechanical properties and seismic mitigation effects of LNR, LRB, and HDR bearings is systematically analyzed, and a solution for rubber isolation bearings to overcome the influence of temperature is proposed. The specific conclusions are as follows:

(1) Temperature exerts the most significant influence on the mechanical properties of HDR bearings. The horizontal equivalent stiffness, yield load, and post-yield stiffness of LNR, LRB, and HDR bearings all decrease with increasing temperature. The impact of temperature on the equivalent damping ratio of LRB bearings is negligible.

(2) For seismic isolation structures employing LNR and HDR bearings, the displacement response of the isolation system increases with rising temperature. The displacement response of the isolation layer with LRB bearings is least affected by temperature, while the displacement response of the seismic isolation system with HDR bearings is most significantly influenced by temperature.

(3) In view of the fact that both the mechanical properties and seismic isolation effect of laminated rubber isolation bearings are related to their operating temperature, a temperature-controlled rubber isolation bearing is innovatively proposed, which enables the rubber bearing to maintain excellent mechanical properties and seismic isolation effect in a relatively wide temperature range.

Author Contributions: C.W. proposed the research concept, formulated the overall research approach, and wrote the manuscript; T.L. reviewed and edited the manuscript; R.X. reviewed and edited the manuscript and provided funding support. All authors have read and agreed to the published version of the manuscript.

Funding: This study was funded by the Training Program for Young Backbone Teachers in Higher Education Institutions of Henan Province (2025GGJS139, 2025GGJS138), the Youth Special Project of Science and Technology Innovation in Zhumadian City (QNZX202506), the Higher Education Teaching Reform Research and Practice Project of Henan Province (2024SJGLX0174), and the National Natural Science Foundation of China (NSFC) (52578583).

Data Availability Statement: The original contributions presented in this study are included in the article. Further inquiries can be directed to the corresponding author.

Conflicts of Interest: The authors declare no conflicts of interest.

References

1. Wang, S.; Tan, P.; Yuan, Y.; Zheng, W.; Jin, S.; Xu, X. Efficacy of 3M-PTGL on low-temperature seismic performance of polyurethane elastomeric bearings for bridges. *Eng. Struct.* **2023**, *294*, 116703. [CrossRef]
2. Losanno, D.; De Domenico, D.; Madera-Sierra, I.E. Experimental testing of full-scale fiber reinforced elastomeric isolators (FREIs) in unbounded configuration. *Eng. Struct.* **2022**, *260*, 114234. [CrossRef]
3. Furukawa, T.; Ito, M.; Izawa, K.; Noori, M.N. System identification of base-isolated building using seismic response data. *J. Eng. Mech.* **2005**, *131*, 268–275. [CrossRef]
4. Li, K.; Shi, W.; Ding, H.; Chen, Z. Research of thermal oxygen ageing on tensile properties of rubber based on Peck-Yeoh model. *Mater. Res. Express* **2021**, *8*, 065303. [CrossRef]
5. Gjorgjiev, I.; Garevski, M. A polynomial analytical model of rubber bearings based on series of tests. *Eng. Struct.* **2013**, *56*, 600–609. [CrossRef]
6. Gallardo, J.A.; de la Llera, J.C.; Restrepo, J.I.; Chen, M. A numerical model for non-linear shear behavior of high damping rubber bearings. *Eng. Struct.* **2023**, *289*, 116234. [CrossRef]
7. Pang, H.; Jiang, T.; Dai, J.; Yang, Y. Study the effects of ambient temperature on full-scale rubber bearings. *Structures* **2025**, *74*, 108535. [CrossRef]

8. Mazza, F. Effects of the long-term behaviour of isolation devices on the seismic response of base-isolated buildings. *Struct. Control. Health Monit.* **2019**, *26*, e2331. [CrossRef]
9. Shen, J.; Akira, I.; Dang, J.; Hamada, Y.; Himeno, T. A multi-layer thermo-mechanical coupling hysteretic model for high damping rubber bearings at low temperature. *Earthq. Eng. Struct. Dyn.* **2024**, *53*, 1028–1047. [CrossRef]
10. Zhang, R.J.; Li, A.Q. Experimental study on temperature dependence of mechanical properties of scaled high-performance rubber bearings. *Compos. Part B* **2020**, *190*, 107932. [CrossRef]
11. Aditya, M.S.; Verma, M.; Priya, C.B.; Yadukrishnan, A.S. Thermo-mechanical response of an elastomeric isolation system using real-time hybrid simulation. *Mech. Time-Depend. Mater.* **2025**, *29*, 24. [CrossRef]
12. Billah, A.M.; Todorov, B. Effects of subfreezing temperature on the seismic response of lead rubber bearing isolated bridge. *Soil Dyn. Earthq. Eng.* **2019**, *126*, 105814. [CrossRef]
13. Xu, X.; Yuan, Y.; Jin, S.; Han, Z.; Liang, C.; Zhu, H. Study on polyurethane elastomer modification for improving low-temperature resistance of high-capacity polyurethane elastomeric bearing for bridges. *Constr. Build. Mater.* **2022**, *347*, 128625. [CrossRef]
14. Xu, G.; Guo, T.; Li, A.; Zhang, R.; Zhu, R.; Liu, F. Influence of ambient temperature on seismic performance of elastomeric isolation structural system. *Structures* **2023**, *55*, 1763–1773. [CrossRef]
15. Cardone, D.; Gesualdi, G. Experimental evaluation of the mechanical behavior of elastomeric materials for seismic applications at different air temperatures. *Int. J. Mech. Sci.* **2012**, *64*, 127–143. [CrossRef]
16. Wang, G.; Du, Y.; Zhang, C.; Li, Y. Mechanism of mechanical properties degradation of rubber isolation bearings at low temperatures. *Structures* **2025**, *71*, 108116. [CrossRef]
17. Candau, N.; Laghmach, R.; Chazeau, L.; Chenal, J.M.; Gauthier, C.; Biben, T.; Munch, E. Influence of strain rate and temperature on the onset of strain induced crystallization in natural rubber. *Eur. Polym. J.* **2015**, *64*, 244–252. [CrossRef]
18. Xue, B.; Lu, W.; Ren, X.; Wen, W. A hysteretic model of lead-rubber bearings considering coupled thermal and mechanical behavior. *J. Build. Eng.* **2025**, *103*, 112118. [CrossRef]
19. Kalpakidis, I.V.; Constantinou, M.C.; Whittaker, A.S. Effects of large cumulative travel on the behavior of lead-rubber seismic isolation bearings. *J. Struct. Eng.* **2010**, *136*, 491–501. [CrossRef]
20. Fu, J.Y.; Cheng, H.; Wang, D.S.; Zhang, R.; Xu, T.T. Temperature-dependent performance of LRBs and its effect on seismic responses of isolated bridges under near-fault earthquake excitations. *Structures* **2022**, *41*, 619–628. [CrossRef]
21. Yasar, C.; Karuk, V.; Kaplan, O.; Cavdar, E.; Ozdemir, G. Amplification in mechanical properties of a lead rubber bearing for various exposure times to low temperature. *Buildings* **2023**, *13*, 478. [CrossRef]
22. Tan, Y.; Dang, J.; Igarashi, A.; Himeno, T.; Hamada, Y. Hysteretic restoring force model of high damping rubber bearings including thermo-mechanical coupled effect. *Eng. Struct.* **2023**, *277*, 115449. [CrossRef]
23. Cardone, D.; Gesualdi, G.; Nigro, D. Effects of air temperature on the cyclic behavior of elastomeric seismic isolators. *Bull. Earthq. Eng.* **2011**, *9*, 1227–1255. [CrossRef]
24. Wang, L.; Yu, L.; Du, X.; Zhang, X.; Li, Z. Seismic response of a pc continuous box girder bridge under extreme ambient temperature. *Sustainability* **2023**, *15*, 14763. [CrossRef]
25. Zheng, W.; Wang, H.; Hao, H.; Bi, K. Superelastic CuAlBe wire-based sliding lead rubber bearings for seismic isolation of bridges in cold regions. *Eng. Struct.* **2021**, *247*, 113102. [CrossRef]
26. Peng, T.; Li, F.; Ma, C. Study on coupling correlation of factors affecting mechanical properties of high-damping rubber plate. *Polymers* **2025**, *17*, 593. [CrossRef] [PubMed]
27. Liu, W.G.; Yang, Q.R.; Zhou, F.L. Temperature properties of natural rubber bearings. *J. Guangzhou Univ. (Nat. Sci. Ed.)* **2002**, *1*, 51–56. (In Chinese)
28. Pang, H.; Jiang, T.; Dai, J.; Yang, Y.; Bai, W. Experimental study of the mechanical properties of full-scale rubber bearings at 23 °C, 0 °C, and −20 °C. *Polymers* **2024**, *16*, 903. [CrossRef]
29. Miyamura, T.; Ohsaki, M.; Fujiwara, J.; Yamamoto, M. Coupled structural and heat conduction FE analysis of laminated high damping rubber bearing. *Earthq. Eng. Struct. Dyn.* **2021**, *50*, 2462–2487. [CrossRef]
30. Shen, C.; Zhou, F.; Cui, J.; Huang, X.; Zhuang, X.; Ma, Y. Dependency test research of mechanical performance of HDR and its parametric value analysis. *Earthq. Eng. Eng. Vib.* **2012**, *32*, 95–103. (In Chinese)
31. Jin, J.M.; Tan, P.; Zhou, F.L. Test study on the equivalent damping ratio of linear natural rubber bearings. *Xi'an Univ. Archit. Technol.* **2009**, *41*, 663–667. (In Chinese)
32. Bandini, P.A.C.; Siqueira, G.H.; Padgett, J.E.; Paultre, P. Seismic performance assessment of a retrofitted bridge with natural rubber isolators in cold weather environments using fragility surfaces. *J. Bridge Eng.* **2022**, *27*, 04022040. [CrossRef]

Disclaimer/Publisher's Note: The statements, opinions and data contained in all publications are solely those of the individual author(s) and contributor(s) and not of MDPI and/or the editor(s). MDPI and/or the editor(s) disclaim responsibility for any injury to people or property resulting from any ideas, methods, instructions or products referred to in the content.